Mini-UAV Attitude Estimation Using an Inertially Stabilized Payload

YAAKOV OSHMAN, Senior Member, IEEE
MICHAEL ISAKOW
Technion–Israel Institute of Technology

A novel method is introduced for autonomous attitude estimation of a mini unmanned aerial vehicle (UAV) carrying an inertially stabilized payload. The method is based on utilizing the outputs of rate gyros normally used to inertially stabilize the payload, and other data that is normally available from conventional aircraft-mounted sensors. A decentralized estimation algorithm is developed, which uses the aircraft/payload mathematical models to bound the estimation errors. Exploiting modern multiprocessor computer technology, the new estimation algorithm comprises two parallel extended Kalman filters (EKFs) and a data fusion algorithm. Real-time experimental tests, incorporating a payload model with real rate gyros mounted on a three-axis flight table, have validated the feasibility of the concept. The theoretical and experimental investigation demonstrates that the estimation algorithm is capable of estimating the attitude angles with an estimation error not exceeding 1 deg, at output rates of 13 Hz, thus constituting a viable substitute for the conventional vertical gyroscope.

Manuscript received October 27, 1997; revised May 12, 1999.

IEEE Log No. T-AES/35/4/09317.

This research was supported by the Department of Research and Development of the Israeli Ministry of Defense and by TAMAM—Precision Instruments Industries.

Authors' address: Technion–Israel Institute of Technology, Department of Aerospace Engineering, Technion City, Haifa 32000, Israel.

I. INTRODUCTION

This paper addresses the problem of attitude determination for low-cost, mini unmanned aerial vehicles (UAVs). Measurements of aircraft attitude angles are essential for its control and navigation. The vertical gyroscope, currently the most common method for determining the aircraft pitch and roll angles, has several disadvantages that cannot be overlooked when designing very small, inexpensive, and possibly even dispensable mini-UAVs. It is acceleration-sensitive, bulky, relatively expensive, and generally has low reliability. The other established method for determining the aircraft attitude is by means of inertial grade sensors, but this method is very expensive and is generally not acceptable for low-cost mini-UAVs. Thus, in the current state-of-the-art, the vertical gyroscope is still mainly used, and, in light of the disadvantages listed above, an attitude determination method which does not rely on its use is highly desirable.

Several works have been reported in the literature, in which an effort was made to determine the aircraft attitude avoiding the use of the vertical gyroscope [1–3]. A paper by Koifman and Merhav [4] presents, to the best of the authors' knowledge, the state-of-the-art in this area, and partly motivated the research reported herein. In that work an attitude reference system was developed, computer-simulated, and experimentally tested in the laboratory, that is able to determine the aircraft angular attitude based on a strapdown orthogonal triad of low-cost low-quality rate gyroscopes. The outputs of the rate gyroscopes drive an extended Kalman filter (EKF), operating in real-time, that assumes a complete knowledge of the nonlinear dynamics model of the aircraft.

In addition to the vertical gyroscope, the inertially stabilized electro-optical payload, which provides visual and other data, is another avionics component playing a major role at the core of modern mini-UAV technology. Although the vertical gyroscope and the electro-optical payload are functionally mutually exclusive within the mini-UAV system, they consist of elements based on similar technological principles: gimbaled motion controlled by torque motors, measurement of inertial angular variables, and measurements of the gimbals' relative angular position. This technological similarity, along with the vast increase in the power of on-board micro-computers in recent years, motivated the main idea investigated herein; namely, to unify the similar functions of the vertical gyroscope and the inertially stabilized payload in one system, thus saving the need to use the vertical gyroscope at the expense of using more computations.

The work presented here can be viewed as a natural, albeit significant, extension of [4]. A real-time attitude estimation algorithm is presented, which

utilizes the output of miniature rate gyroscopes, mounted on the inner gimbal of the payload and used commonly in the framework of the payload inertial stabilization control system, together with other conventional measurements (magnetic heading, relative airspeed, and barometric altitude). Since all sensors needed are normally mounted on the aircraft/payload system, no additional sensors need to be installed. Where the available on-board computing resources do not suffice, the only needed addition to the avionic system is a real-time computer. The following objectives were set for the attitude estimator: 1) it should compare to a vertical gyroscope (of the type commonly used in mini-UAV systems) in terms of attitude accuracy, i.e., its estimation error should not exceed 1 deg, 2) it should be robust, in terms of estimation accuracy, with respect to payload motion and with respect to moderate aircraft and payload parameter variations,[1] and 3) it should be computationally efficient, so as to provide attitude data at an adequate rate for the purposes of control, navigation and display.

The idea underlying this work is that the UAV attitude can be obtained not by directly integrating the outputs of rate gyros, but, rather, by blending the rate gyro outputs with other information sources (i.e., the aircraft dynamics model). As a simple illustration of this idea, consider the following equation, relating the roll angle ϕ of an aircraft in a coordinated turn to its rate of turn Ω and velocity V:

$$\tan\phi = \frac{V}{g}\Omega. \tag{1}$$

Clearly, instead of integrating the output of a roll rate gyro in order to compute the aircraft roll angle, one can directly use the (measurable) rate of turn Ω and velocity V to compute ϕ, thus overcoming the error divergence problem inherently associated with methods based on integrating the outputs of low-grade rate gyros.

Two versions of the estimator are presented. The first is a full-order EKF (FOEKF), which was used in off-line computer simulations. These simulations were part of an extensive study conducted to investigate the feasibility of the proposed idea and the sensitivity of the estimator to payload motion and to aircraft/payload model uncertainties.

In the second phase of the research the idea was tested experimentally, using a real-time version of the filter. The goal of the experimental phase was to demonstrate that the estimator can operate at a sufficiently high rate under conditions as close to real life as possible. Since the FOEKF involved a relatively heavy computational burden, an alternative estimator, tailored for real-time application, was developed. This real-time filter (RTF) is a decentralized estimator, that exploits the loose coupling between the aircraft and the payload. Developed under the principle of maximum a posteriori probability (MAP), it consists of two reduced-order EKFs working in parallel, and a fusion center in which both partial estimates of the two EKFs are merged to yield an improved estimate. Since the decentralized algorithm utilizes two processors working in parallel, as opposed to a conventional, serial implementation of the EKF, it yields a computation time saving of about 50% for the particular problem tested.

The remainder of this paper is organized as follows. In the next section, the mathematical model of the aircraft/payload system is outlined. The FOEKF designed to validate the estimation concept via off-line computer simulations is presented in Section III, along with its simulation results. In Section IV the decentralized estimation algorithm is theoretically developed. Then, in the next section it is applied to the attitude estimation problem, to yield the RTF. The experimental investigation, carried out to investigate the performance of the RTF under almost "real life" conditions, is described in Section VI. Concluding remarks are offered in the last section.

II. AIRCRAFT/PAYLOAD MATHEMATICAL MODEL

In this section a concise description of the mathematical model of the aircraft/payload system is presented.

A. Aircraft Model

The aircraft mathematical model comprises the standard nonlinear six degrees of freedom equations of motion [4, 5]. For the sake of brevity, these equations are not repeated here.

Atmospheric turbulence is modeled using the Dryden mathematical model [6]. The turbulence is represented by the three component gust field $(u_g, v_g, w_g)^T$, where each component is modeled as an airspeed- and altitude-dependent first-order Gauss–Markov process with an unknown mean.

Augmenting the aircraft states with the gust states, the following airframe state vector results

$$x_{a/c} \stackrel{\Delta}{=} (u \quad v \quad w \quad p \quad q \quad r \quad \phi \quad \theta \quad \psi \quad h \quad u_g \quad v_g \quad w_g)^T \tag{2}$$

where u, v, and w are the aircraft velocity components in a body-fixed coordinate system (X_b, Y_b, Z_b); p, q, and r are the airframe angular rates in that coordinate system; ϕ, θ, and ψ are the conventional Euler angles of the airframe with respect to an inertial frame of reference (X_I, Y_I, Z_I) and h is the barometric altitude.

[1]The uncertainty in mini-UAVs stability and control derivatives do not normally exceed 5% of their nominal value, since the small size of mini-UAVs facilitates full-scale wind tunnel testing.

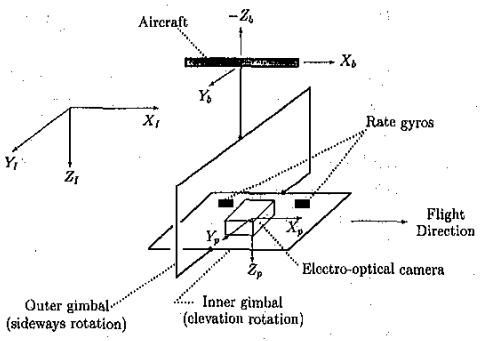

Fig. 1. Two-axis payload gimbal arrangement.

The aircraft control vector comprises the standard elevator, aileron, rudder, and throttle controls, respectively:

$$u_{a/c} \triangleq (\delta_e \quad \delta_a \quad \delta_r \quad \delta_T)^T. \tag{3}$$

The airframe-mounted sensors constitute the following measurement vector:

$$y_{a/c} = (\psi \quad u_r \quad h \quad r)^T \tag{4}$$

where the Euler angle ψ is measured by the aircraft magnetic heading sensor, the relative airspeed component along the body-fixed X_b axis $u_r \triangleq u - u_g$ is measured by the aircraft airspeed sensor, h is measured by the barometric altitude sensor, and r is the aircraft yaw rate, measured by a body-mounted yaw rate gyro.

B. Payload Model

The electro-optical payload assumed in this study is TAMAM's conventional, two-gimbal stabilized day surveillance payload (DSP) [7]. It is noted, however, that the extension of this work to a three-gimbal payload is straightforward. The gimbals are arranged such that the outer gimbal is used for the sideways rotation motion of the payload, while the inner gimbal is used for the elevation rotation. The gimbal arrangement is shown in Fig. 1.

Let (X_p, Y_p, Z_p) denote a Cartesian coordinate system which is fixed to the inner gimbal of the payload. To obtain the attitude of the payload coordinate system, the outer gimbal is first rotated sideways through an angle $\tilde{\psi}$ about the Z_b axis. This yields an intermediate payload-fixed coordinate system, denoted by (X_p', Y_p', Z_p'). Rotating this system through an elevation angle $\tilde{\theta}$ about Y_p' then yields the final attitude of the payload-fixed system.

The electro-optical camera and two rate gyros are mounted on the inner gimbal. The input axis of the first rate gyro is aligned along the payload Y_p axis, while the input axis of the second rate gyro is aligned along the Z_p axis. The contributions of the aircraft roll, pitch and yaw rates to the outputs of the elevation and sideways rate gyros are, respectively

$$q_p^{AC} = -p\sin\tilde{\theta} + q\cos\tilde{\psi} \tag{5a}$$

$$r_p^{AC} = p\cos\tilde{\psi}\sin\tilde{\theta} + q\sin\tilde{\psi}\sin\tilde{\theta} + r\cos\tilde{\theta} \tag{5b}$$

while the angular rates contributed by the gimbal rotations are, respectively

$$q_p^G = \dot{\tilde{\theta}} \tag{6a}$$

$$r_p^G = \dot{\tilde{\psi}}\cos\tilde{\theta}. \tag{6b}$$

Summing the rate contributions from both sources, and assuming small aircraft angular rates and payload elevation angle (which is a realistic assumption for a mini-UAV carrying a downward-looking electro-optical camera), yields the following approximate expressions for the gimbal-mounted rate gyro outputs:

$$q_p \approx \dot{\tilde{\theta}} \tag{7a}$$

$$r_p \approx \dot{\tilde{\psi}} + r. \tag{7b}$$

The payload is inertially stabilized by a control system, using the rate gyro outputs in two separate feedback loops, one for each degree of freedom. The payload gimbals are driven by two torque motors, commanded by the stabilization control system and, potentially, by the ground-based operator.

For the purpose of designing a Kalman filter that estimates the aircraft attitude using sensor outputs from the payload, the payload is next modeled as a dynamic system, which is a simplified version of TAMAM's dynamic model of the DSP [7]. Accordingly, the payload system is mathematically modeled by two uncoupled, first-order inertially stabilized dynamic systems. Denoting the elevation gimbal torque motor command voltage by V_θ, and the payload pitch angle by Θ_p, the transfer function of the closed-loop payload elevation control system is

$$\frac{\dot{\Theta}_p(s)}{V_\theta(s)} = \frac{K_\theta}{s + \tau_\theta}. \tag{8}$$

Similarly, denoting the outer gimbal torque motor command voltage by V_ψ, and the payload yaw angle by Ψ_p, the transfer function of the closed-loop payload sideways motion control system is

$$\frac{\dot{\Psi}_p(s)}{V_\psi(s)} = \frac{K_\psi}{s + \tau_\psi} \tag{9}$$

where K_θ and K_ψ are the control system constant gains. The state vector of the payload is defined as

$$x_p \triangleq (\Theta_p \quad \dot{\Theta}_p \quad \Psi_p \quad \dot{\Psi}_p)^T. \tag{10}$$

The payload control vector comprises the torque motors command voltages

$$u_p = (V_\theta \quad V_\psi)^T. \tag{11}$$

The payload-related measurement vector is

$$y_p = (\tilde{\psi} \quad \tilde{\theta} \quad r_p \quad q_p)^T \tag{12}$$

where $\tilde{\psi}$, the outer gimbal relative sideways rotation angle, and $\tilde{\theta}$, the inner gimbal elevation angle, are usually measured by two low-grade gimbal-mounted resolvers.

Assuming small aircraft pitch and roll angles, a straightforward, albeit cumbersome, analysis shows that

$$\tilde{\theta} \approx \Theta_p \tag{13}$$

$$\tilde{\psi} \approx \Psi_p - \psi \tag{14}$$

so that, under the small angle assumption, (7) yield

$$q_p \approx \dot{\Theta}_p \tag{15}$$

$$r_p \approx \dot{\Psi}_p. \tag{16}$$

C. Augmented System

The total system state and control vectors are defined by augmentation:

$$x_s = (x_{a/c}^T \quad x_p^T)^T, \qquad u_s \triangleq (u_{a/c}^T \quad u_p^T)^T. \tag{17}$$

The dynamic nonlinear equations of motion of the complete aircraft/payload system take the following state space form:

$$\frac{d}{dt}x_s(t) = f[x_s(t), u_s(t)] + Dw_s(t). \tag{18}$$

The process noise $w_s \in \mathbb{R}^5$ comprises the Dryden turbulence model stochastic inputs and the payload torque motors parasitic noise inputs. w_s is assumed to be a Gaussian distributed, zero mean, white noise process with known intensity $Q(t)$. The constant matrix D is the noise distribution matrix.

Augmenting the aircraft measurement vector $y_{a/c}$ by the payload measurement vector y_p yields the total system measurement vector

$$y_s = (y_{a/c}^T \quad y_p^T)^T \tag{19}$$

and the system measurement equation

$$y_s(k) = g[x_s(k)] + v_s(k) \tag{20}$$

where $x_s(k)$ denotes the state vector at time t_k and $v_s(k) \in \mathbb{R}^8$ is a white, zero-mean, Gaussian-distributed measurement noise, possessing the measurement noise covariance $R(k)$.

Based on the system equations (18) and (20), the nonlinear attitude estimator is described next.

III. FULL-ORDER EXTENDED KALMAN FILTER

The first stage of this study consisted of a series of off-line computer simulations, which was performed to validate the viability of the proposed estimation concept. In this section we present the main stages of the design and simulation of an FOEKF, used to estimate the aircraft attitude angles.

Using a discretized version of the system state equations, (18) and (20), a nonlinear EKF was formulated in a straightforward manner [8]. The optimal statistical parameters of the filter (i.e., the covariance matrices $Q(k)$ and $R(k)$) were determined via a filter tuning process, involving a statistical hypothesis testing procedure [9]. The filter update rate was 20 Hz.

An extensive computer simulation study was performed in order to determine the feasibility of the estimation concept. In particular, these simulations were carried out to address the following key points.

Accuracy: The first objective of the simulations was to verify that the estimated aircraft attitude is accurate enough, so as to permit its on-line usage by a typical navigation and control system, i.e., that the estimator accuracy is comparable to that of a conventional, low-cost vertical gyroscope.

Robustness: The problem of algorithm robustness to parameter variations arises since the aircraft parameters (i.e., stability and control derivatives, mass and inertia, etc.) are known only to within some tolerance (albeit small). Therefore, a sensitivity study was performed in order to determine the range of parameter variations for which the algorithm can be considered sufficiently accurate.

Modeling: The third objective of the simulation study was to assess the effects of sensor bias on the estimator accuracy. The objective here was to determine the importance of correctly modeling the sensor bias states.

To assess the attitude estimation quality, several flight conditions were assumed and simulated. The altitude, speed, and bank angle of the aircraft were controlled via three automatic pilots which were designed and programmed as part of the simulation program. The aircraft chosen for the simulations was a small, subsonic, conventionally configured mini-UAV, of the type used in [4].

In the first stage of the simulations, the aircraft parameters were assumed to be perfectly known. The flight conditions were selected so as to span a wide operational envelope of the aircraft. To demonstrate the performance of the estimation algorithm, the results obtained for a typical flight condition, which included a series of coordinated turns, are shown. The total duration of the simulation was 500 s. The payload was perfectly inertially stabilized by its control system, so as to keep its line-of-sight fixed in inertial space. The initial payload relative rotation

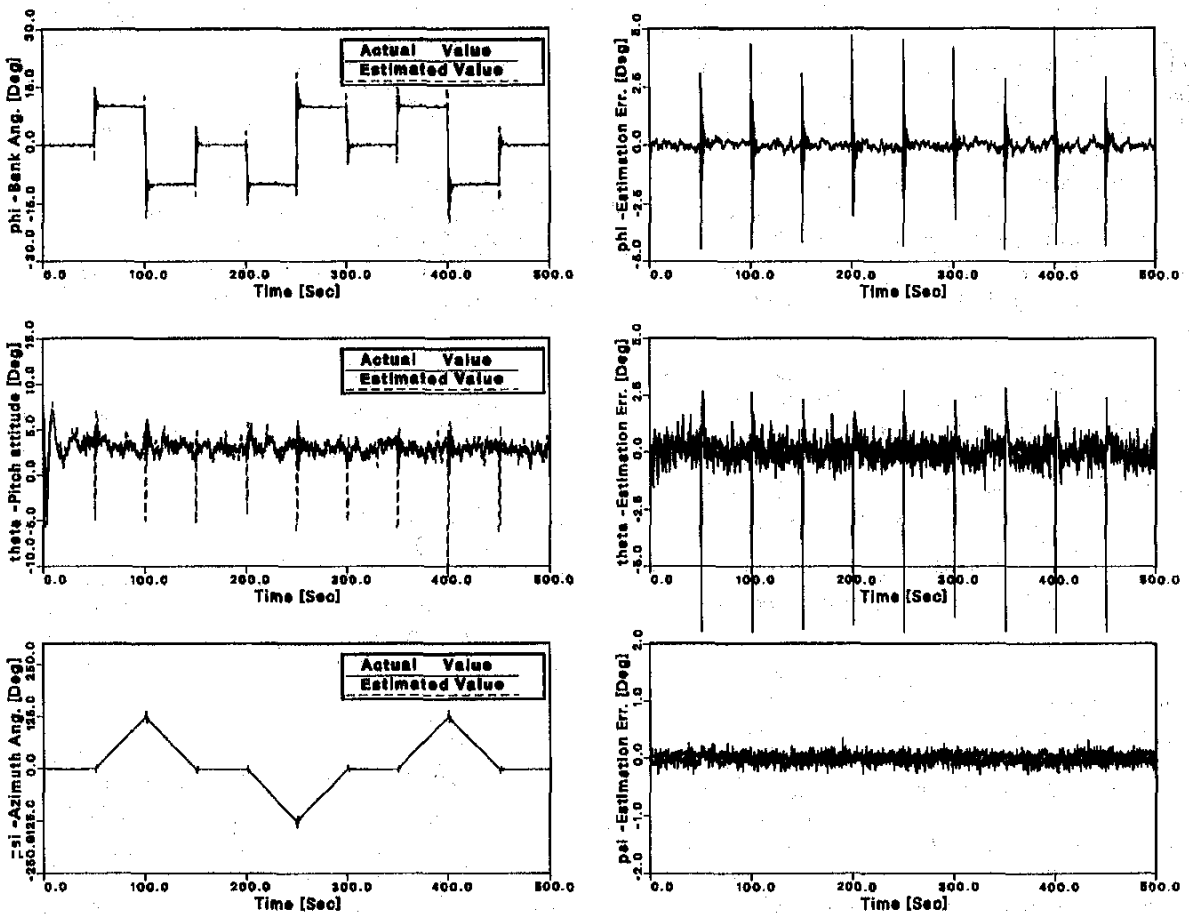

Fig. 2. Attitude angles and their estimation errors using FOEKF in coordinated turn flight, with inertially stabilized payload.

angle were $\tilde{\psi}_0 = 90$ deg and $\tilde{\theta}_0 = 0$ deg. Since the aircraft performed a series of turns, the payload gimbals had to be continuously controlled during the flight, in order to compensate for the airframe motion and to stabilize the camera line-of-sight in inertial space. This flight path was chosen, among others, since it enabled testing the filter performance under mixed-type conditions, involving intervals of straight and level flight, and subsequent periods of coordinated turns which occurred after the filter gain had almost converged to its steady state value. The time histories of the true and estimated attitude angles, and the errors in their estimation, are shown in Fig. 2. As can be observed, the 1σ estimation error values in the azimuth, pitch, and roll angles are below the 1 deg threshold. Notice that along with the excellent filter tracking and convergence, relatively large pitch and roll estimation error spikes arise when the aircraft abruptly changes its bank angle. In real life these excursions are not expected to show due to the fact that mini-UAVs normally perform much milder maneuvers. However, even the appearance of these spikes should not pose any major problem, since they can be easily filtered via a simple low-pass filter.

Numerous other simulations were performed. These included straight and level flights under different turbulence intensities; flights with the payload gimbals positioned close to the gimbal-lock region, i.e., $\tilde{\theta} \approx 90$ deg; "slalom" flights; flights involving sharp turns; and flights in which the payload was operated in some intentional pattern by the ground operator. No substantial sensitivity to the airframe or payload motions was observed. Thus, it was concluded that the attitude angles can be determined by the FOEKF with an accuracy comparable to that normally provided by a conventional vertical gyroscope, i.e., an estimation error not exceeding 1 deg.

In real life it cannot be assumed that the system parameters are perfectly known. Moreover, some of the aircraft parameters normally change during the flight (e.g., the total aircraft mass and the mass distribution). To verify that the FOEKF is robust with respect to changes in these parameters, off-line simulations were run in which the parameters were changed within a range of 10% off their nominal (true) values. Filter sensitivity with respect to changes in the aircraft mass and important aerodynamic

stability derivatives ($C_{L\alpha}, C_{m\alpha}, C_{nr}$) was examined. The simulation results indicated that the filter is not substantially sensitive to parameter variations smaller than 10% of the nominal parameter values, and the resulting estimation error was still below 1 deg.

Finally, the effects of unmodeled sensor bias on the filter performance were investigated. In particular, FOEKF simulations were run under the assumptions of 2 deg bias in the compass reading, 2 m/s bias in the airspeed sensor, and 10 m bias in the barometric altimeter. The conclusions from these simulations are the following.

1) Compass bias could not be estimated by the filter, using the given sensor configuration.

2) Airspeed sensor bias had a minor effect on the estimated pitch angle, and no significant effects on the other attitude angles. Thus, a 5% bias in the airspeed reading caused less than 0.2 deg pitch angle estimation error.

3) A 10 m bias in the barometric altitude reading had no measurable effect on the estimated attitude angles.

These conclusions led to subsequent simplifications in the design of the reduced-order RTF which was implemented in the laboratory experiments.

At the conclusion of the off-line computer simulations, it was determined that the idea was feasible. The FOEKF was able to estimate the attitude angles of the aircraft with an estimation error not exceeding 1 deg, under a wide variety of flight conditions and reasonable parameter variations. The next stage of the research was involved with the implementation of the filter in a manner which would facilitate its on-line operation. This is presented in the following sections.

IV. DECENTRALIZED ESTIMATION

The filter presented in the previous section was designed for a dynamic system of order 17. As is well known, the computational load of a Kalman filter is roughly proportional to the third power of the system order [10]. Since the filter has to be implemented on a mini-UAV with limited computational resources, the relatively large dimension of the system state vector could severely limit the measurement processing rate. Remembering that the estimated attitude angles are needed in real time by the navigation and control systems at a rate typically exceeding 10 Hz, the computational burden could, thus, pose a serious problem. The solution suggested in this work is to implement the estimator via a decentralized scheme, comprised of two smaller-size EKFs working in parallel. The underlying observations leading to the development of this solution were twofold. First, the current state-of-the-art in the computer technology of today makes it quite conceivable to have on-board the aircraft a computer that comprises several processors that can work in parallel. Second, the system under consideration is composed of two subsystems, namely, the aircraft and the payload, which are only loosely dynamically coupled. Hence, the implementation of a separate, reduced-order state estimator for each subsystem provides a natural solution to the aforementioned computational load problem.

In the sequel, the decentralized estimation problem is formulated and solved in a general setting. Then, in the next section, the resulting algorithm is applied to the attitude determination problem.

A. Theoretical Development

We start by partitioning the system state vector as

$$x \triangleq (x_1^T \quad x_2^T)^T \tag{21}$$

where $x \in \mathbb{R}^n$, $x_1 \in \mathbb{R}^{n_1}$, $x_2 \in \mathbb{R}^{n_2}$. The major assumption underlying this partition is that the two state vectors, x_1 and x_2, pertain to two subsystems that are only loosely coupled. Thus, neglecting the coupling between the two subsystems, it is assumed that the following discrete-time, state space models exist:

$$x_1(k+1) = f_1[x_1(k)] + \Gamma_1(k)w_1(k) \tag{22a}$$

$$x_2(k+1) = f_2[x_2(k)] + \Gamma_2(k)w_2(k). \tag{22b}$$

The process noise sequences $\{w_1\}$ and $\{w_2\}$ are assumed to be white, zero mean, Gaussian distributed and with covariance matrices $Q_1(k)$ and $Q_2(k)$, respectively. Moreover, it is also assumed that the measurement vector can be partitioned according to

$$y(k) \triangleq (y_1^T(k) \quad y_2^T(k) \quad y_3^T(k))^T \tag{23}$$

where the three measurement vectors relate to the corresponding partitioned state vectors according to

$$y_1(k) = H_1(k)x_1(k) + v_1(k) \tag{24a}$$

$$y_2(k) = H_2(k)x_2(k) + v_2(k) \tag{24b}$$

$$y_3(k) = H_{3,1}(k)x_1(k) + H_{3,2}(k)x_2(k) + v_3(k). \tag{24c}$$

As can be observed from (24), $y_1 \in \mathbb{R}^{m_1}$ is the measurement vector associated with the state x_1, $y_2 \in \mathbb{R}^{m_2}$ is the measurement vector associated with the state x_2, and $y_3 \in \mathbb{R}^{m_3}$ is the vector comprising the measurements associated with both subsystems. It is assumed that $\{v_1(k)\}$, $\{v_2(k)\}$, and $\{v_3(k)\}$ are mutually uncorrelated, Gaussian-distributed zero-mean white sequences with covariances $R_1(k)$, $R_2(k)$, and $R_3(k)$, respectively.

The decentralized estimation scheme, to be developed in the sequel, is composed of the following components.

1) An EKF that estimates the state vector x_1, using the associated measurement y_1, is denoted as EKF-1.

2) An EKF that estimates the payload state vector x_2, using the associated measurement y_2, is denoted

as EKF-2. The two separate filters, EKF-1 and EKF-2, are designed to work in parallel, on separate processors.

3) A data fusion center, which fuses the estimates resulting from the two EKFs and, at the same time, processes the additional measurement y_3, is the third component. The output of the fusion center is then used to drive the two EKFs in subsequent estimation cycles.

The two EKFs which are designed for the subsystems 1 and 2 are formulated in a straightforward manner [8], based on the system equations (22) and the subsystem measurement equations (24a) and (24b). Hence, to complete the development of the estimator, it remains to develop the data fusion algorithm. This is done in the sequel, based on a MAP principle.

Let $\mathcal{Y}^k$ be the measurement history up to time t_k, i.e., all the measurements processed in estimation stages preceding the current fusion step. That is,

$$\mathcal{Y}^k \triangleq \{y(0), y(1), \ldots, y(k-1), y_1(k), y_2(k)\}. \quad (25)$$

Note that $y_3(k)$ has yet to be processed, which is the task to be performed by the fusion center. For that purpose, the following assumptions are made.

1) The measurement $y_1(k)$ has been processed by EKF-1, yielding the estimate $\bar{x}_1(k \mid k)$ and its error covariance matrix $\overline{P}_1(k \mid k)$. Similarly, $y_2(k)$ has been processed by EKF-2, yielding the estimate $\bar{x}_2(k \mid k)$ and its error covariance matrix $\overline{P}_2(k \mid k)$.

2) The conditional densities $p(x_1(k) \mid \mathcal{Y}^k)$ and $p(x_2(k) \mid \mathcal{Y}^k)$ are independent and Gaussian, with

$$p(x_1(k) \mid \mathcal{Y}^k) \sim \mathcal{N}(\bar{x}_1(k \mid k), \overline{P}_1(k \mid k)) \quad (26a)$$

$$p(x_2(k) \mid \mathcal{Y}^k) \sim \mathcal{N}(\bar{x}_2(k \mid k), \overline{P}_2(k \mid k)). \quad (26b)$$

Obviously, these assumptions constitute, at best, only approximations. They are based on ignoring the loose dynamic coupling between the two subsystems, and the coupling effect of the measurement y_3, processed in previous stages. It is clear, therefore, that the resulting estimator will be suboptimal, and that its performance should be compared with that of the full-order filter.

Using the underlying MAP probability principle, the following optimal estimates are sought

$$\hat{x}(k \mid k) \triangleq (\hat{x}_1^T(k \mid k) \quad \hat{x}_2^T(k \mid k))^T \quad (27)$$

that maximize the conditional density function $p(x(k) \mid \mathcal{Y}^k, y_3(k))$. Using Bayes rule, this density function can be rewritten as

$$p(x(k) \mid \mathcal{Y}^k, y_3(k)) = \frac{p(y_3(k) \mid x(k), \mathcal{Y}^k) p(x(k) \mid \mathcal{Y}^k)}{p(y_3(k) \mid \mathcal{Y}^k)}. \quad (28)$$

Given $x(k)$, $y_3(k)$ is independent of $\mathcal{Y}^k$. Hence

$$p(y_3(k) \mid x(k), \mathcal{Y}^k) = p(y_3(k) \mid x(k)) \quad (29)$$

whence

$$\hat{x}(k \mid k) = \arg\max_{x(k)} p(y_3(k) \mid x(k)) p(x(k) \mid \mathcal{Y}^k). \quad (30)$$

Based on the previous assumptions, $p(x(k) \mid \mathcal{Y}^k)$ is a Gaussian density, with

$$p(x(k) \mid \mathcal{Y}^k) \sim \mathcal{N}\left(\begin{bmatrix} \bar{x}_1(k \mid k) \\ \bar{x}_2(k \mid k) \end{bmatrix}, \begin{bmatrix} \overline{P}_1(k \mid k) & 0 \\ 0 & \overline{P}_2(k \mid k) \end{bmatrix} \right). \quad (31)$$

Also,

$$p(y_3(k) \mid x(k)) \sim \mathcal{N}(H_{3,1}(k) x_1(k) + H_{3,2}(k) x_2(k), R_3(k)). \quad (32)$$

Using (31) and (32) in (30) yields

$$\begin{aligned} \hat{x}(k \mid k) = \arg\min_{x(k)} \Big\{ & \| y_3(k) - H_{3,1}(k) x_1(k) - H_{3,2}(k) x_2(k) \|^2_{R_3^{-1}(k)} \\ & + \| x_1(k) - \bar{x}_1(k \mid k) \|^2_{\overline{P}_1^{-1}(k \mid k)} \\ & + \| x_2(k) - \bar{x}_2(k \mid k) \|^2_{\overline{P}_2^{-1}(k \mid k)} \Big\} \end{aligned} \quad (33)$$

where we used the notation $\|v\|_A^2 \triangleq v^T A v$. Note that the last result means that the a priori estimates, $\bar{x}_1(k \mid k)$ and $\bar{x}_2(k \mid k)$, are treated by the fusion algorithm as additional measurements. Thus, the fusion algorithm optimally blends the information stored in the measurement $y_3(k)$, weighted by its "certainty level," $R_3^{-1}(k)$, and the pseudomeasurements, $\bar{x}_1(k \mid k)$ and $\bar{x}_2(k \mid k)$, weighted by their respective information matrices.

Equation (33) can be rewritten as

$$\begin{aligned} \hat{x}(k \mid k) = \arg\min_{x(k)} \Big\{ & \| R_3^{-1/2}(k) [y_3(k) - H_{3,1}(k) x_1(k) \\ & - H_{3,2}(k) x_2(k)] \|^2 \\ & + \| \overline{P}_1^{-1/2}(k \mid k) [x_1(k) - \bar{x}_1(k \mid k)] \|^2 \\ & + \| \overline{P}_2^{-1/2}(k \mid k) [x_2(k) - \bar{x}_2(k \mid k)] \|^2 \Big\} \end{aligned} \quad (34)$$

where the notation $A^{-1/2}$ stands for the inverse of the square root of A, which is any matrix satisfying

$$A = A^{1/2} (A^{1/2})^T \quad (35)$$

(e.g., the Cholesky upper triangular square root). Define

$$\overline{A}(k) \triangleq \begin{bmatrix} R_3^{-1/2}(k) H_{3,1}(k) & R_3^{-1/2}(k) H_{3,2}(k) \\ \overline{P}_1^{-1/2}(k \mid k) & 0 \\ 0 & \overline{P}_2^{-1/2}(k \mid k) \end{bmatrix} \quad (36)$$

and

$$\bar{b}(k) \triangleq \begin{bmatrix} R_3^{-1/2}(k)y_3(k) \\ \bar{P}_1^{-1/2}(k \mid k)\bar{x}_1(k \mid k) \\ \bar{P}_2^{-1/2}(k \mid k)\bar{x}_2(k \mid k) \end{bmatrix}. \tag{37}$$

Then, (34) can be written as

$$\hat{x}(k \mid k) = \arg\min_{x(k)} \|\bar{A}(k)x(k) - \bar{b}(k)\|^2. \tag{38}$$

Equation (38) is now cast in the form of a standard least squares problem. A variety of methods which are based on orthogonal transformations can be used to solve the problem and yield the estimation error covariance, e.g., QR factorization and singular value decomposition (SVD) [11]. From the theoretical point of view, it is straightforward to show, using standard least squares estimation theory, that the normal equations, leading to the optimal estimate $\hat{x}(k \mid k)$, are

$$\begin{bmatrix} A(k) & C^T(k) \\ C(k) & B(k) \end{bmatrix} \begin{bmatrix} \hat{x}_1(k \mid k) \\ \hat{x}_2(k \mid k) \end{bmatrix} = \begin{bmatrix} \bar{P}_1^{-1}(k \mid k)\bar{x}_1(k \mid k) + H_{3,1}^T(k)R_3^{-1}(k)y_3(k) \\ \bar{P}_2^{-1}(k \mid k)\bar{x}_2(k \mid k) + H_{3,2}^T(k)R_3^{-1}(k)y_3(k) \end{bmatrix} \tag{39}$$

where the following definitions are used

$$A(k) \triangleq \bar{P}_1^{-1}(k \mid k) + H_{3,1}^T(k)R_3^{-1}(k)H_{3,1}(k) \tag{40}$$

$$B(k) \triangleq \bar{P}_2^{-1}(k \mid k) + H_{3,2}^T(k)R_3^{-1}(k)H_{3,2}(k) \tag{41}$$

$$C(k) \triangleq H_{3,2}^T(k)R_3^{-1}(k)H_{3,1}(k). \tag{42}$$

Moreover, the estimation error covariance is

$$\hat{P}(k \mid k) \equiv E[x(k) - \hat{x}(k \mid k)][x(k) - \hat{x}(k \mid k)]^T = \begin{bmatrix} A(k) & C^T(k) \\ C(k) & B(k) \end{bmatrix}^{-1}. \tag{43}$$

It follows that the updated covariance matrix for the partial state vector $x_1(k)$, after performing the fusion, can be computed as the following inverse of the Schur complement of $B(k)$:

$$\hat{P}_1(k \mid k) = [A(k) - C^T(k)B^{-1}(k)C(k)]^{-1}. \tag{44}$$

Similarly, the updated covariance matrix for the partial state vector $x_2(k)$ after the fusion is the following inverse of the Schur complement of $A(k)$:

$$\hat{P}_2(k \mid k) = [B(k) - C(k)A^{-1}(k)C^T(k)]^{-1}. \tag{45}$$

Note that, although the fusion algorithm generates a correlation between the two separate estimates, this correlation is ignored when the fused estimates are fed back to the separate EKFs. This approximation contributes to the suboptimality of the overall estimation scheme.

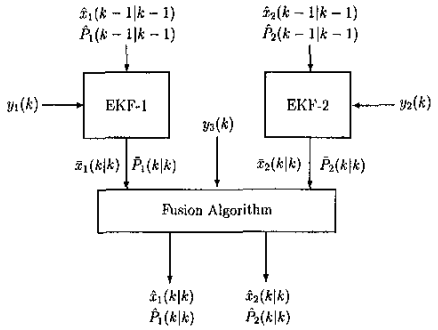

Fig. 3. Decentralized estimation scheme.

The decentralized estimation algorithm is shown schematically in Fig. 3.

V. REAL-TIME ESTIMATOR

In this section, the previously developed decentralized estimator is applied to the problem of attitude angles estimation. The resulting filter, denoted as RTF, is then compared with the FOEKF.

A. Order Reduction

A few changes were made in the system mathematical model, prior to the application of the decentralized estimator. Listed below are changes made based on conclusions drawn from the off-line FOEKF simulations.

1) Since the mathematical model of the aircraft renders the azimuth angle unobservable, the estimator cannot improve the estimation quality of this variable over the quality of the compass reading. Hence, the aircraft azimuth angle ψ was deleted from the aircraft state vector and the compass reading was directly used by the filter.

2) The barometric altitude h was also deleted from the aircraft state vector, since it was proved that a bias in the measurement of this variable does not substantially affect the attitude estimation error. The measured altitude, although containing measurement noise, was directly utilized (without filtering). It should be noted, that in practice it is customary to pass the altimeter reading through a low-pass filter whose time constant is 30 s; it is anticipated that such passive filtration will only improve the results.

3) Instead of estimating the absolute aircraft speed components and the gust components, the relative airspeed velocity components were estimated, i.e.,

$$u_r \triangleq u - u_g, \qquad v_r \triangleq v - v_g, \qquad w_r \triangleq w - w_g. \tag{46}$$

Having reduced the model order, we are left with the following state and measurement vectors

$$x_1 = (u_r \quad v_r \quad w_r \quad p \quad q \quad r \quad \phi \quad \theta)^T \tag{47a}$$

$$x_2 = (\Theta_p \quad \dot{\Theta}_p \quad \Psi_p \quad \dot{\Psi}_p)^T \tag{47b}$$

where x_1 is the state vector of the aircraft and x_2 is the state vector of the payload. The measurement vector is partitioned according to

$$y_1 = (u_r \quad r)^T, \qquad y_2 = (\tilde{\theta} \quad q_p)^T, \qquad y_3 = (\tilde{\psi} \quad r_p)^T \tag{48}$$

where y_1 comprises the measurements associated with the aircraft state variables, y_2 comprises the measurements associated with the payload state variables, and y_3 comprises the measurements associated with both state vectors.

Cast in the form of (47) and (48), the present formulation allows the application of the previously developed decentralized estimation algorithm.

B. Multirate Implementation

In practice, the decentralized estimator was implemented via a direct solution of the normal equations. For that purpose, the inverses of the covariances $\overline{P}_1(k \mid k)$ and $\overline{P}_2(k \mid k)$ need to be computed at each data fusion step. To reduce the real-time computational load, the algorithm was implemented in a multirate manner, where the inverse of $\overline{P}_1(k \mid k)$ (which is a symmetric, positive definite 8×8 matrix) was computed at a low rate of one inversion per four data fusions. Numerous computer simulations demonstrated that this multirate implementation (and even implementations with lower inversion rates) did not cause any substantial degradation in the filter performance. In the sequel, the reduced-order decentralized, multirate filter is denoted as the RTF.

C. RTF/FOEKF Comparison

Off-line simulations of the RTF were performed in order to evaluate its performance versus the performance of the FOEKF and to assess its robustness with respect to variations in the model parameters. In Fig. 4 the performance of the two filters is compared for the same flight condition. The aircraft is flying a straight and level flight, and the payload is inertially stabilized in a position such that the camera line-of-sight is perpendicular to the ground. Fig. 4 shows a comparison of the estimation errors of the pitch and roll angles, as yielded by the RTF and FOEKF for measurements acquired from the real sensors mounted on the laboratory flight table (described in the following section). As can be expected, the performance of the FOEKF is somewhat better than that of the RTF. However, the RTF performance is still acceptable, and its estimation error is below the 1 deg threshold.

Simulations performed to evaluate the RTF robustness have demonstrated that it was more sensitive than the FOEKF to variations in the model parameters. The results of these simulations are summarized in Tables I and II. However, the sensitivity observed was still deemed acceptable, especially since, as previously mentioned, the parameters of a mini-UAV are normally known with high accuracy (due to the small size of the airframe, which allows for wind tunnel testing of the full scale mini-UAV model).

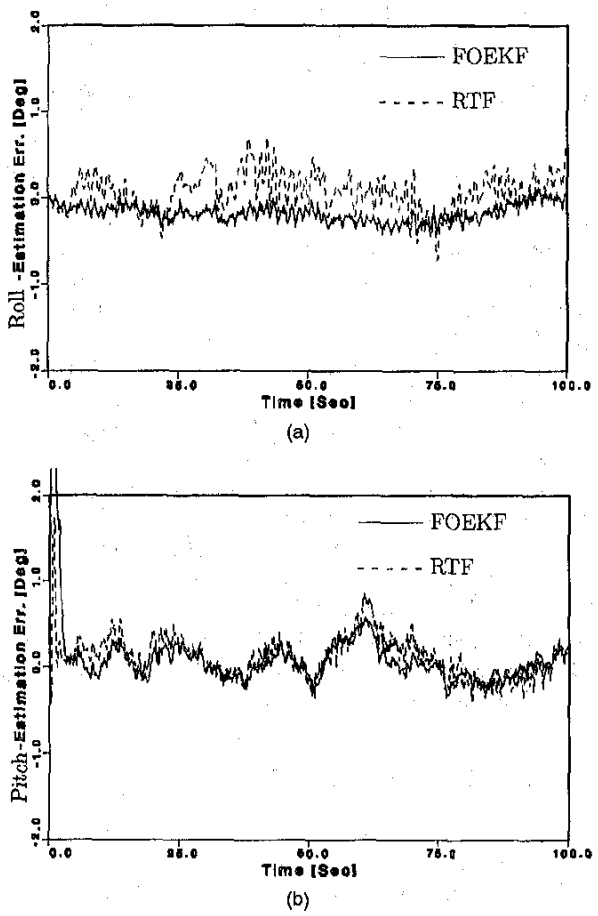

Fig. 4. RTF/FOEKF estimation error comparison in straight and level flight, with inertially stabilized payload. (a) Roll angle. (b) Pitch angle.

TABLE I
FOEKF Sensitivity

Parameter	Mass	$C_{L\alpha}$	$C_{m\alpha}$	C_{nr}
Parameter Variation (%)	20	10	10	10
Estimation Error (deg)	$\Delta\theta = 0.2$	$\Delta\theta = 0.3$	$\Delta\theta = 0.2$	$\Delta\phi = 0.1$

TABLE II
RTF Sensitivity

Parameter	Mass	$C_{L\alpha}$	$C_{m\alpha}$	C_{nr}
Parameter Variation (%)	5	5	5	10
Estimation Error (deg)	$\Delta\theta = 1$	$\Delta\theta \approx 0.3$	$\Delta\theta = 0.7$	$\Delta\phi = 0.1$

D. RTF/FOEKF Computational Load Comparison

The computational load associated with the implementation of the Kalman filter is given by [10]

$$\text{LOAD(KF)} = 2n^3 + 3n^2 + (1.5n^2 + 4.5n)m \quad \text{FLOPS} \tag{49}$$

per one time update/measurement update cycle, where n is the dimension of the state and m is the dimension of the measurement vector. Hence, the computational burden associated with one cycle of the FOEKF ($n = 12$, $m = 6$) is about 5508 FLOPS. Since the RTF is implemented on a three-processor machine, the computations associated with EKF-1 and EKF-2 are performed simultaneously. Hence, the computational load associated with the RTF can be estimated by adding the load of EKF-1 ($n = 8$, $m = 2$), which is 1480 FLOPS, and the work load of the fusion algorithm. Using the operation counts given in [12], the computational load of the fusion step is estimated at 1100 FLOPS. Thus, it is concluded that the implementation of the RTF rendered a computation time saving of about 50% relative to the serial implementation of the FOEKF.

VI. EXPERIMENTAL INVESTIGATION

To validate the proposed estimation concept and to demonstrate the performance of the decentralized estimator in the presence of unmodeled sensor noises and uncertainties, an extensive experimental investigation was carried out in the laboratory. This investigation is presented in the sequel.

A. Experimental Setup

The experimental setup used for this stage of the investigation comprised the following components.

1) First is a high-precision computer-controlled three-axis flight table. The flight table angular motion about each axis is unlimited, and the angular position of each axis is measured by an optical sensor having a resolution of 0.0055 deg.

2) Second is a two-axis payload model, simulating a conventional electro-optical payload commonly used in today's mini-UAVs. The payload gimbals are actuated by two dc torque motors. Two Helipot 6153 linear potentiometers measure the gimbals relative rotation angles ($\tilde{\theta}$ and $\tilde{\psi}$). The payload is controlled via a lead-lag compensator, that stabilizes the line-of-sight of the payload in inertial space and enables commanding the payload to perform a specified motion pattern. The control system utilizes the output of the rate gyros that are mounted on the inner gimbal of the payload. The flight table and the payload model are depicted in Fig. 5.

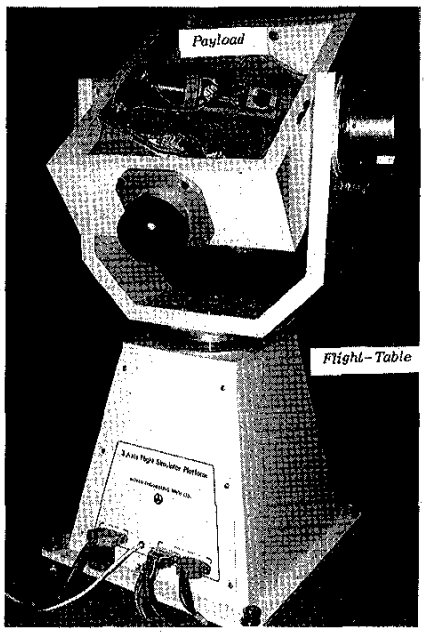

Fig. 5. Flight table and payload model.

3) Third is the two TAMAM 2417 rate gyros that are mounted on the inner gimbal of the payload, and a third identical rate gyro that is mounted on the yaw gimbal of the flight table (the "aircraft body"). These rate gyros have a measurement range of ±150 deg/s, and a resolution of 0.015 deg/s.

4) Fourth is a Motorola VME System 1131 real-time computer that controls the flight table via a special purpose communication board. The System 1131 computer is based on a 16 MHz MC68020 CPU/MC68881 FPU combination. The communication board, used to interface the computer and the flight table, is based on an 8 MHz MC68010 CPU and three 12 bit analog-to-digital converters that sample the readings of the three rate gyros.

5) Fifth is a Motorola VME System 1147 multiprocessor real-time computer, that is used for the implementation of the decentralized estimation algorithm. The computer consists of a central processing board that is based on a 20 MHz MC68030 CPU/MC68882 FPU combination, and three target boards, each based on a MC68020 CPU, that can be run in parallel.

B. Procedure

Prior to performing the real-time experiments, the parameters of the payload subsystem (equations (8) and (9)) were identified from the measured step response of the payload. The RTF described in the previous section was implemented on the

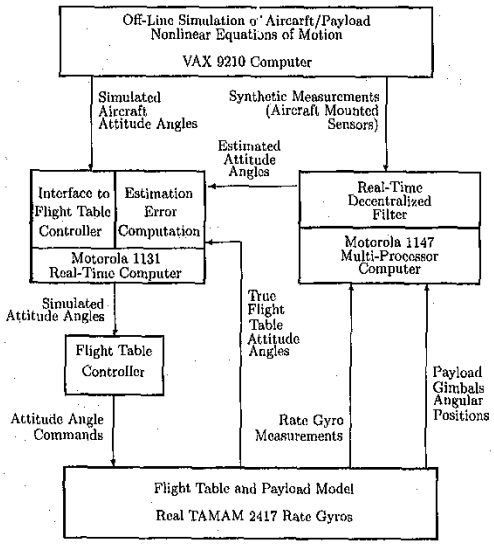

Fig. 6. Experimental setup.

Motorola System 1147 computer, exploiting the computer parallel processing capability. The statistical parameters of the filter were optimally tuned using a hypothesis testing procedure (see Section III). The measurement processing rate of the RTF was 13.3 Hz, which is an adequate rate for the purposes of control, navigation, and display. The experiments were performed in accordance with the flow diagram shown in Fig. 6. The main stages of an on-line experiment are the following.

1) An off-line simulation program is run on a VAX 9210 computer. By solving the nonlinear six degrees of freedom equations, time histories of the following variables are computed: a) the attitude angles of the aircraft, b) the (noise contaminated) outputs of the airspeed sensor, the barometric altitude sensor and the compass, and c) the aircraft control surfaces deflections as well as the throttle position.

2) The time histories of the aircraft attitude angles are transferred to the Motorola System 1131 computer, forming the commands to the flight table. During the flight table operation, the true attitude angles are sampled and stored for a later comparison with the estimated angles.

3) The rate gyros mounted on the payload and on the flight table and the payload-mounted potentiometers are sampled during the flight table operation. Their outputs, along with the synthetic measurements produced by the prior off-line simulation, drive the RTF which is implemented on the Motorola System 1147 computer. The RTF processes the data acquired and computes in real-time the estimated attitude angles of the flight table. These angles are finally compared with the real flight table angles, for an evaluation of the real estimation errors.

Similarly to the off-line FOEKF simulations, several flight conditions were run, spanning a wide operational envelope for the aircraft/payload system. Fig. 7 shows the results obtained for a flight condition involving a combination of coordinated turns and intervals of straight and level flight. The payload was inertially stabilized during the total duration of the flight, which was 300 s. This flight condition was similar to that of Fig. 2, which represented an off-line FOEKF computer simulation. Note, however, that in the FOEKF simulation, represented by Fig. 2, imperfections of the flight table and payload model uncertainty did not play a role. On the other hand, these factors, as well as the sensor nonlinear characteristics and unmodeled noise, were in effect present during the real-time experiment represented by Fig. 7. Nevertheless, as can be observed from this figure, the estimation quality obtained was similar to that obtained during the off-line simulation. For both the pitch and roll angles, the estimation errors remained bounded during the flight, not exceeding 1 deg. Similar results were obtained for other flight conditions, including slalom flights and flights in which the payload was commanded to perform specified motion patterns.

VII. CONCLUSIONS

An innovative decentralized estimation scheme was presented for the determination of the attitude of a mini-UAV. The method utilizes the outputs of on-board existing sensors, including rate gyros normally mounted on an inertially stabilized electro-optical payload. The algorithm was tested via computer simulations and laboratory experiments. It was demonstrated that the aircraft attitude can be estimated on-line at an accuracy comparable to that of a conventional vertical gyroscope, thus meeting the typical requirements of mini-UAV control and navigation systems. Sufficient robustness with respect to aircraft parameter uncertainty was demonstrated, and the filter was shown to perform well under a variety of flight conditions representing a wide operational envelope. The conclusion from this study is that the proposed estimation concept constitutes a feasible substitute, or at least a viable backup system, for the bulky and expensive vertical gyroscope, which is typically characterized by its low reliability.

ACKNOWLEDGMENTS

Helpful discussions and suggestions of Professor S. J. Merhav of the Department of Aerospace Engineering are gratefully acknowledged.

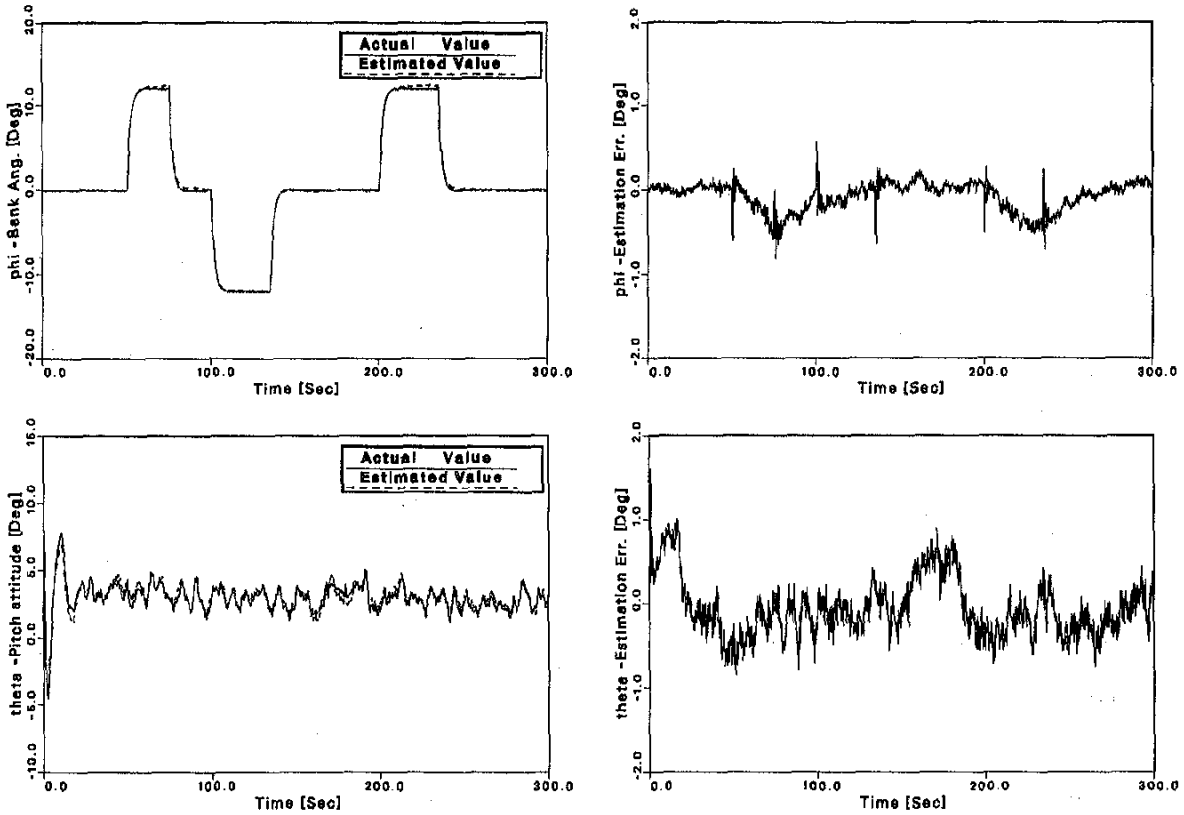

Fig. 7. Roll and pitch angles and their estimation errors using RTF in online laboratory experiment. Coordinated turn flight, with inertially stabilized payload.

REFERENCES

[1] Bar-Itzhack, I. Y., and Ziv, I. (1986)
Frequency and time domain design of a strapdown vertical determination system.
Paper 86-2148, AIAA, New York, 1986.

[2] Bryson, A. E., Jr. (1978)
Kalman filter divergence and aircraft motion estimators.
Journal of Guidance and Control, **1**, 1 (1978), 71–78.

[3] Grunwald, A. J., Wahnon, E., and Merhav, S. J. (1983)
Estimation of vehicle attitude and flight-path angles from low-cost rate gyro measurements.
In *Proceedings of the 25th Israel Annual Conference on Aviation and Astronautics*, Haifa, Israel, Feb. 1983, 121–127.

[4] Koifman, M., and Merhav, S. J. (1991)
Autonomously aided strapdown attitude reference system.
Journal of Guidance, Control, and Dynamics, **14**, 6 (1991), 1164–1172.

[5] Blakelock, J. H. (1991)
Automatic Control of Aircraft and Missiles.
New York: Wiley, 1991.

[6] Heffley, R. K. (1977)
A study of key features of random atmospheric disturbance models for the approach flight phase.
In *Proceedings of the AIAA Atmosphere Flight Mechanics Conference*, 1977, 219–228.

[7] Feldhorn, Z. (1987)
Stabilized day surveillance payload (DSP)—Technical description.
Technical report A-0972.0002.00.19-1021-4, Israel Aircraft Industries, Electronics Division/TAMAM Precision Instruments Industries, Yahud, Israel, Aug. 1987.

[8] Mendel, J. M. (1987)
Lessons in Digital Estimation Theory.
Englewood Cliffs, NJ: Prentice-Hall, 1987.

[9] Bar-Shalom, Y., and Fortmann, T. E. (1988)
Tracking and Data Association.
New York: Academic Press, 1988.

[10] Bierman, G. J. (1973)
A comparison of discrete linear filtering algorithms.
IEEE Transactions on Aerospace and Electronic Systems, **AES-9**, 1 (1973), 28–37.

[11] Lawson, C. L., and Hanson, R. J. (1974)
Solving Least Squares Problems.
Englewood Cliffs, NJ: Prentice-Hall, 1974.

[12] Dongarra, J. J., Moler, C. B., Bunch, J. R., and Stewart, G. W. (1979)
LINPACK User's Guide.
SIAM, Philadelphia, 1979.

Yaakov Oshman (A'96—SM'97) received the B.Sc. (Summa cum laude) and the D.Sc. degrees, both in aeronautical engineering, from the Technion–Israel Institute of Technology, Haifa, Israel, in 1975 and 1986, respectively.

From 1975 to 1981 he was with the Israeli Air Force, where he worked in the areas of structural dynamics and flutter analysis and flight testing. In 1987 he was a Research Associate at the Department of Mechanical and Aerospace Engineering at the State University of New York at Buffalo, where he was, in 1988, a Visiting Professor. Since 1989 he has been with the Department of Aerospace Engineering at the Technion–Israel Institute of Technology, where he is currently an Associate Professor. During the 1996/1997 and 1997/1998 academic years he spent a sabbatical with the Guidance, Navigation and Control Center of NASA's Goddard Space Flight Center, where he worked in research and development of spacecraft attitude estimation algorithms. His research interests are in advanced optimal estimation and control methods and their application in aerospace systems.

Dr. Oshman is an Associate Fellow of the AIAA.

Michael Isakow received the B.Sc. (cum laude) and M.Sc. degrees, both in aerospace engineering, and the MBA degree, from the Technion–Israel Institute of Technology, Haifa, Israel, in 1989, 1992, and 1996, respectively.

From 1992 to 1997 he was with Israel Aircraft Industries (Tamam Division) where he worked in the areas of advanced navigation and inertial technologies for use in air, land, sea, and space platforms, specializing in the integration of inertial navigation systems with the Global Positioning System (GPS). In 1997, he joined Cimatron Ltd., a leading developer of integrated CAD/CAM solutions, where he is currently the European Regional Manager.